

Influence of Electron-Withdrawing Substituents on the Electronic Structure of Oxidized Ni and Cu Salen Complexes

Linus Chiang[†], Khrystyna Herasymchuk[†], Fabrice Thomas[§], Tim Storr^{†*}

[†] Department of Chemistry, Simon Fraser University, Burnaby, British Columbia, V5A 1S6, Canada

[§] Département de Chimie Moléculaire, Chimie Inorganique Redox (CIRE), UMR-5250, Université Grenoble Alpes, BP 53, 38041 Grenoble Cedex 9, France

Supporting Information Placeholder

ABSTRACT: Nickel ($\text{Ni}(\text{Sal}^{\text{CF}_3})$) and copper ($\text{Cu}(\text{Sal}^{\text{CF}_3})$) complexes of an electron-poor salen ligand were prepared, and their one-electron oxidized counterparts were studied using an array of spectroscopic and theoretical methods. The electrochemistry of both complexes exhibited quasi-reversible redox processes at higher potentials in comparison to the $\text{M}(\text{Sal}^{\text{R}})$ ($\text{R} = \text{tBu}$, OMe , NMe_2) analogues, in line with the electron-withdrawing nature of the *para*- CF_3 substituent. Chemical oxidation, monitored by UV-Vis-NIR spectroscopy, afforded their corresponding one-electron oxidized products. Ligand-based oxidation was observed for $[\text{Ni}(\text{Sal}^{\text{CF}_3})]^{+\bullet}$, as evidenced by sharp NIR transitions in the UV-Vis-NIR spectrum and a broad isotropic signal at $g = 2.067$ by solution EPR spectroscopy. Such sharp NIR transitions observed for $[\text{Ni}(\text{Sal}^{\text{CF}_3})]^{+\bullet}$ are indicative of a delocalized electronic structure, which is in good agreement with electrochemical measurements and DFT calculations. In addition, the increased Lewis acidity of $[\text{Ni}(\text{Sal}^{\text{CF}_3})]^{+\bullet}$, evident from the EPR g -value and DFT calculations, was further quantified by the binding affinity of axial ligands to $[\text{Ni}(\text{Sal}^{\text{CF}_3})]^{+\bullet}$. For $[\text{Cu}(\text{Sal}^{\text{CF}_3})]^{+\bullet}$, an intense LMCT band at 18700 cm^{-1} in the UV-Vis-NIR spectrum was observed, which is diagnostic for the formation of a Cu^{III} species [*J. Am. Chem. Soc.*, **2008**, *130*, 15448 – 15459]. The Cu^{III} character for $[\text{Cu}(\text{Sal}^{\text{CF}_3})]^{+\bullet}$ is further confirmed by ^{19}F NMR analysis. Taken together, these results show that the electron-deficient salen ligand $\text{H}_2\text{Sal}^{\text{CF}_3}$ increases the Lewis acidity of the coordinating metal center.

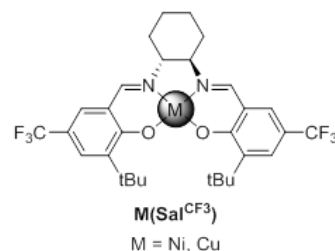
1. Introduction

Transition metal complexes incorporating redox-active ligands are of significant current interest,¹ drawing inspiration from enzymatic systems such as galactose oxidase² and cytochrome P450.³ Reports have documented the pro-radical nature of ligands such as dioxolenes,⁴ dithiolenes,⁵ phenolates,^{2b,6} *o*-phenylenediamines,⁷ amidophenolates,⁸ 1,2-diimines,⁹ and salens.^{1a} This research has greatly improved the understanding of the interaction between transition metal ions and pro-radical ligands, and stimulated transition metal catalyst development incorporating redox-active ligands.^{1,8b,c,9i,10}

The relative ordering of the metal and ligand frontier orbitals dictates whether a metal complex ($\text{M}^{\text{n+}}\text{L}$) will become a ligand-radical complex ($[\text{M}^{\text{n+}}\text{L}]^{+\bullet}$) or a high-valent metal complex ($[\text{M}^{(\text{n+1})}\text{L}]^{+\bullet}$) upon oxidation. Minor changes to the system through solvent/temperature variations or addition of exogenous ligands is sufficient in shifting the locus of oxidation in certain cases.^{4,11} One area of recent focus by our group and others is the redox

activity and electronic structure of tetradentate salen (**Sal**) ligands (salen is a common abbreviation for N_2O_2 bis-Schiff-base bis-phenolate ligands).^{2b,12} Salen ligands have been extensively studied due to their modular synthesis, ability to stabilize many metals in different oxidation states, and versatility as catalysts.¹³ As an example, one-electron oxidized $\text{Ni}^{\text{II}}(\text{Sal})$ derivatives exist in the ligand radical form $[\text{Ni}^{\text{II}}(\text{Sal})]^{+\bullet}$ in solution and the solid state, where ligand electronic tuning via *para*-ring substituent variation influences the degree of delocalization of the ligand radical.^{12c} The addition of exogenous ligands such as DMF or pyridine to $[\text{Ni}^{\text{II}}(\text{Sal})]^{+\bullet}$ results in the shifting of the oxidation locus to the octahedral $[\text{Ni}^{\text{III}}(\text{Sal})(\text{D})_2]^{+\bullet}$ form ($\text{D} =$ axial donor ligand).^{12g,n,q,14} Recent work on $\text{Co}^{\text{II}}(\text{Sal})$ systems has shown that the relative donating abilities of the axial ligands dictates the formation of $[\text{Co}^{\text{II}}(\text{Sal})(\text{D})_x]^{+\bullet}$ or $[\text{Co}^{\text{III}}(\text{Sal})(\text{D})_x]^{+\bullet}$ ($x = 1$ or 2).^{12s,15}

Chart 1. Nickel ($\text{Ni}(\text{Sal}^{\text{CF}_3})$) and copper ($\text{Cu}(\text{Sal}^{\text{CF}_3})$) complexes.



In this work, we investigate the electronic structure of oxidized nickel ($\text{Ni}(\text{Sal}^{\text{CF}_3})$) and copper ($\text{Cu}(\text{Sal}^{\text{CF}_3})$) complexes with electron-withdrawing CF_3 substituents in the *para* position (Chart 1) to determine if electron-withdrawing moieties promote metal-based versus ligand-based oxidation. Due to the geometric preferences of Ni and Cu, the factors governing the locus of oxidation differ. For example, while Ni^{III} d^7 complexes are usually stabilized in an octahedral environment, a square-planar ligand geometry is much preferred for Cu^{III} complexes. Previous research focusing on square-planar $\text{Ni}^{\text{II}}(\text{Sal}^{\text{R}})$ complexes found that the use of electron-donating *para*-ring substituents (i.e. tBu , SR , OMe , NMe_2) promotes ligand radical formation at low oxidation potentials.^{12c,o} Interestingly, oxidation of four-coordinate square-planar Ni^{II} complexes employing diamido-diphenolate ligands,¹⁶ *o*-phenylenedioxamidates and related ligands,^{15c,17} and dipeptides¹⁸ afford Ni^{III} species likely due to the tetra-anionic nature of the ligands. Will dianionic $\text{M}(\text{Sal}^{\text{CF}_3})$ complexes also support a Ni^{III} oxidation state in a square-planar ligand environment?

For Cu, the majority of Cu^{III} complexes reported employ anionic ligands such as carboxylates, thiolates, deprotonated amides, car-

bamates, and N-confused porphyrins. Recent interest in the stabilization of Cu^{III} complexes arises from the isolation of Cu^{III} intermediates in organocopper chemistry,¹⁹ and the synthesis and reactivity of bis(μ -oxo)dicopper(III) complexes.²⁰ Oxidation of the Cu^{II}(Sal^R) system employing *t*Bu *para*-ring substituents affords a Cu^{III} complex in the solid state, yet in solution a reversible spin-equilibrium exists between the ligand radical species [Cu^{II}(Sal^R)]⁺ and high valent metal form [Cu^{III}(Sal)]⁺.^{12f} Employing OMe *para*-ring substituents, however, affords a ligand radical species upon oxidation under all conditions investigated.^{12q} These studies highlight the effect of salen ligand electronics in dictating the electronic structure of their oxidized forms. Herein, we describe the electronic structure of oxidized M(Sal^{CF3}) (M = Ni, Cu) using experimental and theoretical methods. Oxidized [Ni(Sal^{CF3})]⁺ is demonstrated to exist as a delocalized ligand radical with considerable metal ion participation in the singularly occupied molecular orbital (SOMO), while oxidized [Cu(Sal^{CF3})]⁺ exists as a Cu^{III} complex in solution and the solid state.

2. Experimental Section

2.1 Materials and Methods. All chemicals used were of the highest grade available and were further purified whenever necessary.²¹ 2-*tert*-butyl-4-trifluoromethyl phenol was prepared from commercially available 4-trifluoromethyl phenol by reported procedures.²² The tris(2,4-dibromophenyl)aminium hexafluoroantimonate radical chemical oxidant N(C₆H₃Br₂)₃SbF₆ ($E_{1/2} = 1.14$ V, MeCN)²³ was synthesized according to published protocols.^{14,24} Electronic spectra were obtained on a Cary 5000 spectrophotometer with a custom-designed immersion fiber-optic probe with variable path-length (1 and 10 mm; Hellma, Inc.). Constant temperatures were maintained by a dry ice/acetone bath. Solvent contraction was accounted for in all variable-temperature studies. Affinity constants were obtained by refinement of the UV-Vis titration data of the complexes with pyridine in CH₂Cl₂. Data fitting was completed using SPECFIT software. Cyclic voltammetry (CV) was performed on a PAR-263A potentiometer, equipped with an Ag wire reference electrode, a platinum disk working electrode and a Pt counter electrode with ⁿBu₄NClO₄ (0.1 M) solutions in CH₂Cl₂. Decamethylferrocene was used as an internal standard.²⁵ ¹H, ¹³C and ¹⁹F NMR spectra were recorded on a Bruker AV-500 instrument. Mass spectra (ESI positive ion or ESI negative ion) were obtained on an Agilent 6210 TOF ESI-MS instrument. Elemental analyses (C, H, N) were performed by Mr. Paul Mulyk at Simon Fraser University on a Carlo Erba EA1110 CHN elemental analyzer. All EPR spectra were collected using a Bruker EMXplus spectrometer operating with a premium X-band (~9.5 GHz) microwave bridge. Low temperature measurements of frozen solutions used a Bruker helium temperature-control system and a continuous flow cryostat. Samples for X-band measurements were placed in 4 mm outer-diameter sample tubes with sample volumes of ~300 μ L. Spectra at 195 K were collected in capillary tubes, which were placed inside a standard 4 mm EPR tube.

2.2 X-ray Structure Determination. Single crystal X-ray crystallographic analysis of Ni(Sal^{CF3}) and Cu(Sal^{CF3}) was performed on a Bruker X8 APEX II diffractometer with graphite monochromated Mo-K α radiation. An orange block (Ni(Sal^{CF3})) or a dark purple prism (Cu(Sal^{CF3})) crystal was mounted on a glass fibre. The data were collected at 150 \pm 0.1 K to a maximum 2 θ value of 55.0°. Data were collected in a series of ϕ and ω in 0.50° widths with 10.0 second exposures. The crystal-to-detector distance was 50 mm. The structure was solved by direct methods (SIR92)²⁶ and refined by least-squares procedures using CRYSTALS (v14.40b)²⁷ or ShelXle.²⁸ All non-hydrogen atoms were refined anisotropically. All C-H hydrogen atoms were placed in calculated positions but were not refined. All crystal structure plots were produced using ORTEP-3 and rendered with

POV-Ray (v.3.6.2). A summary of the crystal data and experimental parameters for structure determinations are given in Table 1.

2.3 Oxidation Protocol. Under an inert atmosphere at 195 K, 500 μ L of a CH₂Cl₂ solution of the metal complex (4.6 mM) was added to 3.0 mL of CH₂Cl₂. Monitored by UV-Vis-NIR, a saturated solution of N(C₆H₃Br₂)₃SbF₆ in CH₂Cl₂ was added in 60 μ L additions resulting in clean conversion to the respective one-electron oxidized species.

2.4 X-ray Photoelectron Spectroscopy. Solid samples of the oxidized species were prepared under an inert atmosphere. The oxidized samples were prepared by dissolving the neutral compounds in CH₂Cl₂, then cooled to 233 K, where N(C₆H₃Br₂)₃SbF₆ was added in one portion. Solvent was immediately evacuated, where the color between the solution and resultant solid is maintained. X-ray photoelectron spectra were obtained using a Kratos Analytical Axis ULTRA spectrometer containing a DLD detector. The solid samples were loaded onto the carbon tape under inert atmosphere and the auto-z correction was done using F(1s) binding energy. The X-ray excitation source was at 15 kV and 10 mA. All spectra were referenced to the C(1s) peak (284.2 eV).

2.5 Calculations. Geometry optimizations were performed using the Gaussian 09 program (Revision D.01),²⁹ the B3LYP³⁰ functional with a polarized continuum model (PCM) for CH₂Cl₂ (dielectric $\epsilon = 8.94$)³¹, and the 6-31G(d) basis set on all atoms. This combination of functional and basis set has been previously used for structurally similar salen complexes, providing good matches to experimental metrical parameters.^{12b,d,e} A symmetric structure was used as a starting point for all geometry optimizations. Frequency calculations at the same level of theory confirmed that the optimized structures were located at a minimum on the potential energy surface. Single point calculations for the Ni complexes were performed using the B3LYP³⁰ functional with a PCM for CH₂Cl₂³¹, and the TZVP basis set of Ahlrichs on all atoms.³² The intensities of the 30 lowest-energy electronic transitions for [Ni(Sal)^{CF3}]⁺ were calculated by TD-DFT³³ at the B3LYP/TZVP level with a PCM for CH₂Cl₂. The above calculations were also completed using the CAM-B3LYP³⁴ functional for comparison. Single point calculations for energetic analysis of the Cu complexes were performed using the BLYP³⁵ functional with a PCM for CH₂Cl₂³¹, and the TZVP basis set of Ahlrichs on all atoms.³² AOMix³⁶ was used for determining atomic orbital compositions employing Mulliken Population Analysis.

2.6 Synthesis. **2.6.1. 3-*tert*-butyl-5-trifluoromethylsalicylaldehyde (I).** To a solution of 2-*tert*-butyl-4-trifluoromethyl phenol (1.5 g, 6.9 mmol) in trifluoroacetic acid (30 mL) was added hexamethylenetetramine (1.06 g, 7.6 mmol). The reaction mixture was stirred at reflux for 16 hours, and then it was cooled to room temperature and water (30 mL) was added. This solution was cooled and extracted with CH₂Cl₂ (3 x 50 mL), and the organic phase was dried over Na₂SO₄, and the filtrate was concentrated *in vacuo*. The crude product was subject to flash column chromatography using 4:1 CHCl₃ : Hexanes as the eluent to afford a pale yellow oil as 3-*tert*-butyl-5-trifluoromethylsalicylaldehyde. Yield: 430 mg, 25%. ¹H NMR (CDCl₃, 400 MHz): $\delta = 12.11$ (s, 1H, OH), 9.92 (s, 1H, CHO), 7.71-7.70 (m, 2H, Ar-H), 1.44 (s, 9H, *t*-Bu); ¹³C NMR (CDCl₃, 100 MHz): $\delta = 196.7, 163.7, 140.0, 130.5$ (³J(C,F) = 3 Hz), 129.4 (³J(C,F) = 4 Hz), 124.0 (¹J(C,F) = 271 Hz), 121.8 (²J(C,F) = 33 Hz), 119.9, 35.3, 29.1. MS (ESI negative mode): m/z (%): 245.08 (100) [I+H]⁻.

2.6.2. (N,N'-bis(3-*tert*-butyl-5-trifluoromethylsalicylidene))-trans-1,2-cyclohexanediamine (H₂(Sal^{CF3})). To a solution of *trans*-1,2-cyclohexanediamine (71 mg, 0.6 mmol) dissolved in MeOH (3 mL) was added 3-*tert*-butyl-5-trifluoromethyl-2-hydroxybenz-

aldehyde (305 mg, 1.2 mmol) in MeOH (3 mL). The reaction mixture was stirred at room temperature for 16 hours, during which time a light yellow precipitate formed. The solid was filtered and washed with cold MeOH. Yield: 330 mg (93%). ^1H NMR (CDCl_3): δ = 8.30 (s, 2H, NCH), 7.44-7.45 (d, 2H, Ar-H, J = 2.0 Hz), 7.25-7.26 (d, 2H, Ar-H, J = 2.0 Hz), 3.35-3.42 (m, 2H, CH), 2.02-2.05 (m, 2H, CH_2), 1.88-1.96 (m, 2H, CH_2), 1.74-1.82 (m, 2H, CH_2), 1.45-1.55 (m, 2H, CH_2), 1.40 (s, 18H, *t*-Bu). ^{13}C NMR (CDCl_3 , 100 MHz): δ = 165.1, 163.2, 138.7, 127.0, ($^3J_{\text{C-F}}$: 4 Hz), 126.2 ($^2J_{\text{C-F}}$: 3 Hz), 124.5 (CF_3 , $^2J_{\text{C-F}}$: 271 Hz), 120.0, 117.8, 72.3, 35.1, 32.9, 29.1, 24.3; ^{19}F NMR (CDCl_3 , 560 MHz): δ = -62.8. MS (ESI): m/z (%): 571.27 (100) [$\text{H}_2(\text{Sal}^{\text{CF}_3}) + \text{H}$] $^+$. Elemental Analysis: calculated (%) for $\text{C}_{30}\text{H}_{36}\text{N}_2\text{O}_2\text{F}_6$: C 63.15, H 6.36, N 4.91; Found (%): C 63.50, H 6.53, N 5.12.

2.6.3. (*N,N'*-bis(3-*tert*-butyl-5-trifluoromethylsalicylidene))-*trans*-1,2-cyclohexanediamine Nickel(II) ($\text{Ni}(\text{Sal}^{\text{CF}_3})$). To a solution of $\text{H}_2(\text{Sal}^{\text{CF}_3})$ (50 mg, 0.09 mmol) in Et_2O (2 mL), was added $\text{Ni}(\text{OAc})_2 \cdot 4\text{H}_2\text{O}$ (22 mg, 0.09 mmol) in MeOH (2 mL). NEt_3 (25 μL , 0.18 mmol) was added, and the resulting solution was stirred at room temperature overnight during which time an orange precipitate formed, which was collected by filtration and washed with cold methanol. The crude material was recrystallized in 1:1 CH_2Cl_2 : MeOH to afford orange crystals of $\text{Ni}(\text{Sal}^{\text{CF}_3})$. Yield: 22 mg (40%). ^{19}F NMR (CDCl_3 , 560 MHz): δ = -62.5. MS (ESI): m/z (%): 627.20 (100) [$\text{Ni}(\text{Sal}^{\text{CF}_3}) + \text{H}$] $^+$. Elemental Analysis: calculated (%) for $\text{C}_{30}\text{H}_{34}\text{N}_2\text{O}_2\text{F}_6\text{Ni}$: C 57.44, H 5.46, N 4.47; Found (%): C 57.82, H 5.19, N 4.54.

2.6.4. (*N,N'*-bis(3-*tert*-butyl-5-trifluoromethylsalicylidene))-*trans*-1,2-cyclohexanediamine Copper(II) ($\text{Cu}(\text{Sal}^{\text{CF}_3})$). To a solution of $\text{H}_2(\text{Sal}^{\text{CF}_3})$ (100 mg, 0.18 mmol) in MeOH (2 mL), was added $\text{Cu}(\text{OAc})_2 \cdot \text{H}_2\text{O}$ (35 mg, 0.18 mmol) in MeOH (2 mL). The resulting solution was stirred at room temperature overnight during which time a dark purple precipitate formed, which was collected by filtration and washed with cold methanol. The crude material was recrystallized in 1:1 CH_2Cl_2 : MeOH to afford dark purple crystals. Yield: 60 mg (54%). ^{19}F NMR (CDCl_3 , 560 MHz): δ = -64.4. MS (ESI): m/z (%): 632.19 (100) [$\text{Cu}(\text{Sal}^{\text{CF}_3}) + \text{H}$] $^+$. Elemental Analysis: calculated (%) for $\text{C}_{30}\text{H}_{34}\text{N}_2\text{O}_2\text{F}_6\text{Cu}$: C 57.00, H 5.42, N 4.43; Found (%): C 57.09, H 5.39, N 4.64.

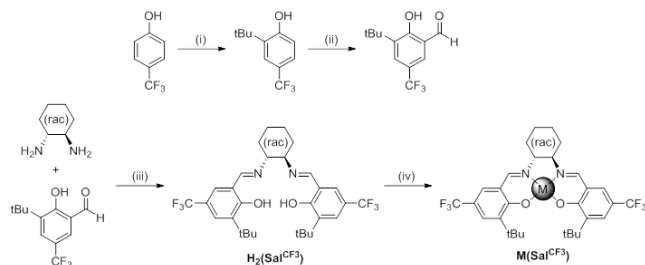
3. Results and Analysis

3.1 Synthesis and Solid State Characterization of Ligands and Complexes. The ligand $\text{H}_2(\text{Sal}^{\text{CF}_3})$ was synthesized by condensation of *trans*-1,2-cyclohexanediamine in the presence of two equivalents of 3-*tert*-butyl-5-trifluoromethyl-2-hydroxybenzaldehyde, which was prepared by the *tert*-butylation of the commercially available 4-trifluoromethylphenol, followed by a Duff formylation reaction. $\text{Ni}(\text{Sal}^{\text{CF}_3})$ and $\text{Cu}(\text{Sal}^{\text{CF}_3})$ were synthesized by reacting $\text{H}_2(\text{Sal}^{\text{CF}_3})$ with the corresponding metal acetate salts ($\text{Ni}(\text{OAc})_2 \cdot 4\text{H}_2\text{O}$ and $\text{Cu}(\text{OAc})_2 \cdot \text{H}_2\text{O}$) under aerobic conditions (Scheme 1). Two equivalents of NEt_3 were added to all metallation reactions. X-ray quality crystals of $\text{Ni}(\text{Sal}^{\text{CF}_3})$, and $\text{Cu}(\text{Sal}^{\text{CF}_3})$ were grown by slow diffusion of MeOH into a concentrated CH_2Cl_2 solution of the compounds.

3.2 X-ray analysis of $\text{Ni}(\text{Sal}^{\text{CF}_3})$ and $\text{Cu}(\text{Sal}^{\text{CF}_3})$. The molecular structures of $\text{Ni}(\text{Sal}^{\text{CF}_3})$ and $\text{Cu}(\text{Sal}^{\text{CF}_3})$ are presented in Figure S1 and Figure 1, respectively, and select crystallographic data for $\text{Cu}(\text{Sal}^{\text{CF}_3})$ is shown in Table 1. A high *R*-value (11.1%) for the X-ray data of $\text{Ni}(\text{Sal}^{\text{CF}_3})$ arises from a second disordered molecule of $\text{Ni}(\text{Sal}^{\text{CF}_3})$ in the unit cell, and thus bond lengths could not be accurately determined. The solid state structure for the two compounds exhibit a slightly distorted square planar geometry with the expected N_2O_2 coordination sphere from the ligand, with the distortion likely due to the sterically demand-

ing *ortho*-*t*Bu substituents. The C-O bond length of the phenolate is often used to evaluate the oxidation state of the ligand.

Scheme 1. Synthetic scheme for $\text{H}_2(\text{Sal}^{\text{CF}_3})$ and $\text{M}(\text{Sal}^{\text{CF}_3})$.^a



^a(i) 9:1 $^1\text{BuOH}$: MeOH, H_2SO_4 , 74%; (ii) Hexamethylenetetramine, CF_3COOH , 25%; (iii) 0.5 equiv. *trans*-1,2-cyclohexanediamine, MeOH, 93%; (iv) $\text{M}(\text{OAc})_2$, MeOH, Ni: 40%, Cu: 54%.

Table 1. Selected crystallographic data for $\text{Cu}(\text{Sal}^{\text{CF}_3})$.

$\text{Cu}(\text{Sal}^{\text{CF}_3})$	
Formula	$\text{C}_{30}\text{H}_{34}\text{F}_6\text{N}_2\text{O}_2\text{Cu}$
Formula weight	632.14
space group	$\text{P2}_1/\text{n}$
<i>a</i> (Å)	8.3007(7)
<i>b</i> (Å)	17.9066(14)
<i>c</i> (Å)	19.9819(16)
α (°)	90
β (°)	98.9040(15)
γ (°)	90
<i>V</i> [Å ³]	2934.3(4)
<i>Z</i> , <i>D</i> _{calc} [g/cm ³]	4
<i>T</i> (K)	150
ρ_{caled} (g cm ⁻³)	1.431
λ (Å)	0.71073
μ (cm ⁻¹)	0.812
<i>R</i> indices ^a with <i>I</i> > 2σ(<i>I</i>) (data)	5351
w <i>R</i> ₂	0.1626
<i>R</i> ₁	0.0440
Goodness-of-fits on <i>F</i> ²	1.509

^a Goodness-of-fit on *F*.

$\text{Cu}(\text{Sal}^{\text{CF}_3})$ displayed C-O bond distances consistent with a phenolate moiety, in line with other $\text{Cu}(\text{Sal}^{\text{R}})$ complexes,^{12q,37} and indicating the dianionic nature of the complex. Overall, the coordination sphere bond distances for $\text{Cu}(\text{Sal}^{\text{CF}_3})$ were found to be slightly longer in comparison to other reported $\text{Cu}(\text{Sal}^{\text{R}})$ derivatives, suggesting phenolates bearing the CF_3 moiety have lower donating ability in comparison to analogues with a *para*-*t*Bu group. This is further illustrated by the shorter coordination bond distances for salen complexes with an electron-rich OMe *para*-*para*-substituent, in comparison to the *t*Bu analogue.^{12q}

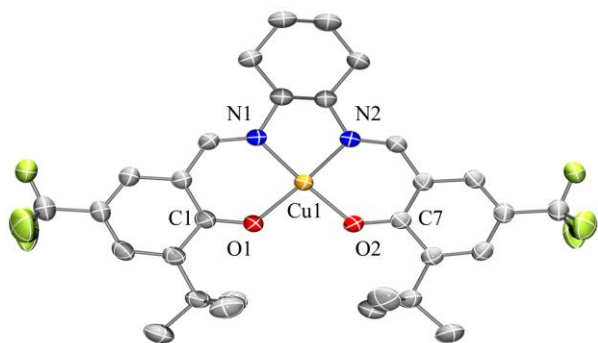


Figure 1. ORTEP plot of $\text{Cu}(\text{Sal}^{\text{CF}_3})$ (50% probability) using POV-Ray, excluding hydrogen atoms. Selected interatomic distances [Å] and angles [°]: Cu(1)-N(1): 1.938, Cu(1)-N(2): 1.939, Cu(1)-O(1): 1.901, Cu(1)-O(2): 1.895, C(1)-O(1): 1.295, C(7)-O(2): 1.297; Angles: N(1)-Cu(1)-N(2): 84.2, N(2)-Cu(1)-O(2): 93.2, O(1)-Cu(1)-O(2): 90.6, N(1)-Cu(1)-O(1): 92.7, N(1)-Cu(1)-O(2): 173.4, O(1)-Cu(1)-N(2): 172.5.

3.3 Electrochemistry. Redox processes for $\text{M}(\text{Sal}^{\text{CF}_3})$ were probed by cyclic voltammetry (CV) in CH_2Cl_2 by using tetra-*n*-butylammonium perchlorate (${}^n\text{Bu}_4\text{NClO}_4$) as the supporting electrolyte. Two quasi-reversible one-electron oxidation waves are observed for $\text{Ni}(\text{Sal}^{\text{CF}_3})$ as previously observed for other $\text{Ni}(\text{Sal}^{\text{R}})$ complexes (Figure 2, Table 2).^{12c,38}

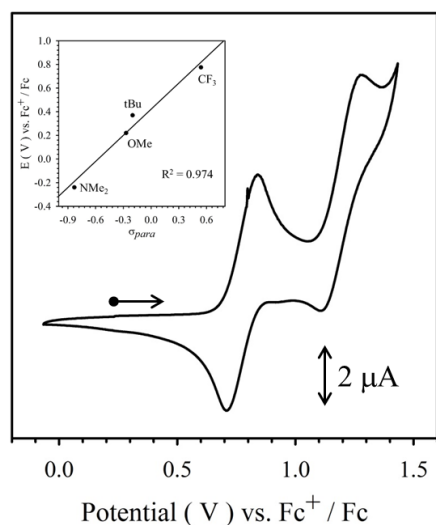


Figure 2. Cyclic voltammogram of $\text{Ni}(\text{Sal}^{\text{CF}_3})$. Inset: Hammett plot of the oxidation potentials of $\text{Ni}(\text{Sal}^{\text{R}})$ vs. σ_{para} of the *para*-ring substituents. Conditions: 1.5 mM complex, 0.1 M ${}^n\text{Bu}_4\text{NClO}_4$, scan rate 100 mV s^{-1} , CH_2Cl_2 , 298 K.

The redox potentials for $\text{Ni}(\text{Sal}^{\text{R}})$ versus Fc^+/Fc are in line with the electron-donating abilities of the *para*-ring substituents,^{12c} which is reflected in the plot between first oxidation potential against Hammett constants (σ_{para}).³⁹ A linear correlation ($R^2 = 0.974$), demonstrates that the oxidation potential is predominantly affected by the relative donating ability of the *para*-ring substituents (Figure 2 inset). Both the first and second redox processes for $\text{Ni}(\text{Sal}^{\text{R}})$ vary by *ca.* 1 V in the series (Table 2). In addition, the difference between the first and second oxidation potentials ($\Delta E_{1/2}$) and comproportionation constant (K_c) of the one-electron oxidized complexes, calculated using Eq. 1-3, are also reported in Table 2, which provides insight regarding the degree of electronic coupling between the two redox-active phenolates in $[\text{Ni}(\text{Sal}^{\text{CF}_3})]^{+}$.⁴⁰ Both $\Delta E_{1/2}$ and K_c values for $[\text{Ni}(\text{Sal}^{\text{CF}_3})]^{+}$ sug-

gest a delocalized ligand radical electronic structure, which is further supported by theoretical analysis (*vide supra*).

$$[\text{ML}] + [\text{ML}^{**}] \leftrightarrow 2[\text{ML}^*] \quad (1)$$

$$K_c = \frac{[\text{ML}^*]^2}{[\text{ML}][\text{ML}^{**}]} \quad (2)$$

$$K_c = \exp\left(\frac{\Delta E_{\text{ox}} F}{RT}\right) \quad (3)$$

Table 2. Redox potentials of $\text{Ni}(\text{Sal}^{\text{R}})$ versus Fc^+/Fc .^a

Compound	$E_{1/2}^1$ (V)	$E_{1/2}^2$ (V)	ΔE_{ox} ($E_{1/2}^2 - E_{1/2}^1$) (V)	K_c
$\text{Ni}(\text{Sal}^{\text{NMe}_2})$ ^b	-0.24 (0.14)	-0.08 (0.14)	0.16	2.9×10^3
$\text{Ni}(\text{Sal}^{\text{OMe}})$ ^b	0.22 (0.14)	0.59 (0.14)	0.37	1.0×10^8
$\text{Ni}(\text{Sal}^{\text{tBu}})$ ^b	0.37 (0.14)	0.85 (0.14)	0.48	2.4×10^{10}
$\text{Ni}(\text{Sal}^{\text{CF}_3})$ ^c	0.78 (0.13)	1.19 (0.17)	0.38 ^b	1.7×10^8

^a Peak-to-peak differences in brackets ($|E_{\text{pa}} - E_{\text{pc}}|$ in V). Peak-to-peak difference for the Fc^+/Fc couple at 233 K is *ca.* 0.13 V, while at 298 K it is *ca.* 0.12 V.

^b Cyclic voltammetry performed at 233 K, ref [12c]

^c Cyclic voltammetry performed at 298 K.

Two quasi-reversible one-electron oxidation waves were observed for $\text{Cu}(\text{Sal}^{\text{CF}_3})$ (Table 3, Figure S2). The redox processes for $\text{Cu}(\text{Sal}^{\text{CF}_3})$ occur at considerably higher potentials in comparison to $\text{Cu}(\text{Sal}^{\text{tBu}})$ and $\text{Cu}(\text{Sal}^{\text{OMe}})$,^{12q,37} as expected based on the trends observed for $\text{Ni}(\text{Sal}^{\text{R}})$.^{12c} Interestingly, it has been reported that the one-electron oxidation of $\text{Cu}(\text{Sal}^{\text{tBu}})$ affords a Cu^{III} species in the solid state, which is in equilibrium with a Cu^{II} -phenoxyl radical species in solution.^{12f} The locus of oxidation is strongly dependent on temperature, highlighting the similarity in energy between the two electronic states. Conversely, the one-electron oxidation of the more electron rich OMe derivative $\text{Cu}(\text{Sal}^{\text{OMe}})$ results in a Cu^{II} -phenoxyl radical species at all temperatures.^{12q} Thus, the electron-withdrawing properties of the CF_3 moiety is expected to lower the energy of the ligand-based HOMO, thereby stabilizing the formation of a Cu^{III} species (*vide infra*). In addition, an irreversible reduction wave was observed at -2.06 V in the CV spectrum, similar reduction processes have been observed for other Cu^{II} -Schiff base complexes indicating reduction to their respective Cu^{I} forms.⁴¹ Similar to the oxidation processes, the *para*-ring substituents in such salen systems can also tune the $\text{Cu}^{\text{II}}/\text{Cu}^{\text{I}}$ reduction potential.^{41c}

Table 3. Redox potentials of $\text{Cu}(\text{Sal}^{\text{R}})$ complexes versus Fc^+/Fc .^a

Compound	$E_{1/2}^1$ (V)	$E_{1/2}^2$ (V)
$\text{Cu}(\text{Sal}^{\text{OMe}})$ ^b	0.28	0.44
$\text{Cu}(\text{Sal}^{\text{tBu}})$ ^c	0.45	0.65
$\text{Cu}(\text{Sal}^{\text{CF}_3})$ ^d	0.74 (0.16)	1.28 (0.16)

^a Peak-to-peak differences in brackets ($|E_{\text{pa}} - E_{\text{pc}}|$ in V). Peak-to-peak difference for the Fc^+/Fc couple at 233 K is *ca.* 0.13 V, while at 298 K it is *ca.* 0.12 V.

^b Cyclic voltammetry performed at 233 K, ref [12q].

^c Cyclic voltammetry performed at 233 K, ref [37].

^d Cyclic voltammetry performed at 298 K.

3.4 Electronic Spectroscopy. *3.4.1. Chemical oxidation of Ni(Sal^{CF3}).* The electronic absorption spectrum of Ni(Sal^{CF3}) is typical of low-spin d⁸ square-planar Ni^{II} bis-phenolate salen complexes (Figure 3).^{12c,q} While no absorption was observed at energies lower than 20000 cm⁻¹ for the neutral form, two intense NIR transitions were observed upon oxidation. These sharp and intense NIR bands for [Ni(Sal^{CF3})]⁺⁺ are observed at similar energies to those of [Ni(Sal^{tBu})]⁺⁺ (tBu: $\nu = 4700$ cm⁻¹, $\epsilon = 21600$ M⁻¹ cm⁻¹, $\nu = 9100$ cm⁻¹, $\epsilon = 7200$ M⁻¹ cm⁻¹; CF₃: $\nu = 4900$ cm⁻¹, $\epsilon = 16200$ M⁻¹ cm⁻¹, $\nu = 8600$ cm⁻¹, $\epsilon = 13100$ M⁻¹ cm⁻¹). Indeed, the band shapes for both [Ni(Sal^{tBu})]⁺⁺ and [Ni(Sal^{CF3})]⁺⁺ are quite similar, suggesting that both oxidized species are Class III delocalized systems by the Robin-Day classification.⁴² While the stability of the oxidized species precluded its isolation for further crystallographic characterization ($t_{1/2}$ (298 K): *ca.* 80 minutes), the delocalized electronic structure is supported by EPR data and DFT calculations (*vide infra*). Interestingly, while [Ni(Sal^{tBu})]⁺⁺ and [Ni(Sal^{CF3})]⁺⁺ both exhibit delocalized electronic structures, the relative intensity of their respective NIR features differ, and is further explored by TD-DFT calculations (*vide infra*).

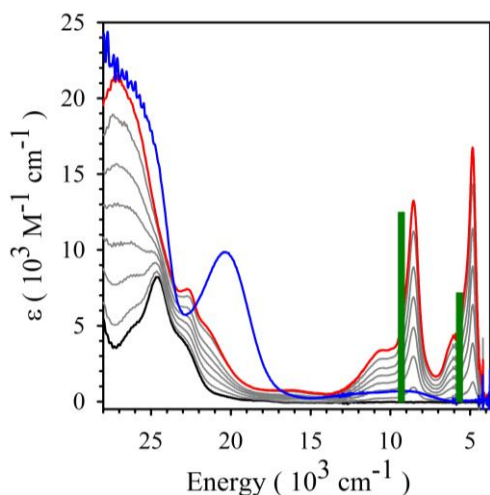


Figure 3. Electronic spectra of Ni(Sal^{CF3}) (black), [Ni(Sal^{CF3})]⁺⁺ (red) and [Ni^{III}(Sal^{CF3})(py)₂]⁺ (blue). Intermediate gray lines measured during the oxidation titration with N(C₆H₃Br₂)₃SbF₆ in CH₂Cl₂ at 198 K. Green bars represent transitions predicted by TD-DFT.

3.4.2. Pyridine binding to [Ni(Sal^{CF3})]⁺⁺. The addition of 30 equivalents of pyridine to [Ni(Sal^{CF3})]⁺⁺ in solution results in the loss of the NIR transitions and emergence of a new transition at 20300 cm⁻¹ (Blue spectrum, Figure 3). This spectral pattern has been previously observed for the axial binding of two pyridines to [Ni(Sal^{tBu})]⁺⁺ to form [Ni^{III}(Sal^{tBu})(py)₂]⁺, with an accompanying shift in the locus of oxidation from the ligand to metal.^{12g} Binding affinities of pyridine to [Ni(Sal^R)]⁺⁺ (R = tBu, CF₃) were determined by incremental addition of pyridine to a solution of the oxidized species (Figure S3-4), and the resultant data was fit according to Equation 4:

$$\log \beta_2 = \frac{[\text{Ni}^{\text{III}}(\text{Sal}^{\text{R}})(\text{py})_2]^+}{[\text{Ni}(\text{Sal}^{\text{R}})]^{++}[\text{py}]^2} \quad (4)$$

At 198 K, [Ni(Sal^{tBu})]⁺⁺ and [Ni(Sal^{CF3})]⁺⁺ exhibited log β₂ values of 7.7 ± 0.2 M⁻² and 12.4 ± 1.1 M⁻², respectively. The higher binding constant for [Ni(Sal^{CF3})]⁺⁺ reflects the expected increase in electrophilicity of the Ni center chelated by an electron poor ligand. The formation of [Ni(Sal^{CF3})]⁺⁺ and [Ni^{III}(Sal^{CF3})(py)₂]⁺ is further evidenced by EPR spectroscopy (*vide infra*).

3.4.3. Chemical oxidation of Cu(Sal^{CF3}). The electronic absorption spectrum of Cu(Sal^{CF3}) is typical of low-spin d⁹ square-planar Cu^{II} bis-phenolate salen complexes, with an intense charge transfer transition at 28000 cm⁻¹ ($\epsilon = 12500$ M⁻¹ cm⁻¹) and a weak d-d transition at 17600 cm⁻¹ ($\epsilon = 600$ M⁻¹ cm⁻¹) (Figure 4).^{12f,q} The oxidation of Cu(Sal^{CF3}) leads to the appearance of two new bands at 18700 cm⁻¹ ($\epsilon = 17300$ M⁻¹ cm⁻¹) and 6300 cm⁻¹ ($\epsilon = 1400$ M⁻¹ cm⁻¹), which are in line with a previous report.^{12f} The emergence of the intense band at *ca.* 18000 cm⁻¹ has been linked to the formation of a Cu^{III} species (LMCT transition), as observed for [Cu(Sal^{tBu})]⁺ at low temperature ($\epsilon = 14000$ M⁻¹ cm⁻¹).^{12f} In comparison, no such band was observed for [Cu(Sal^{OMe})]⁺, in which the formation of a Cu^{II}-phenoxy radical species is favored due to the electron-donating ability of the *para*-OMe moiety.^{12q} In addition, the intensity of the band at *ca.* 18000 cm⁻¹ for [Cu(Sal^{tBu})]⁺ is reduced by 50% upon warming from 198 K to 298 K, signifying a reversible temperature-dependent equilibrium between a Cu^{III} species at low temperature and a Cu^{II}-phenoxy radical species at room temperature.^{12f} This effect could not be probed for [Cu(Sal^{CF3})]⁺ above 233 K due to its thermal instability at 273 K, as evident by the irreversible decrease in its LMCT transition with warming (Figure S5).

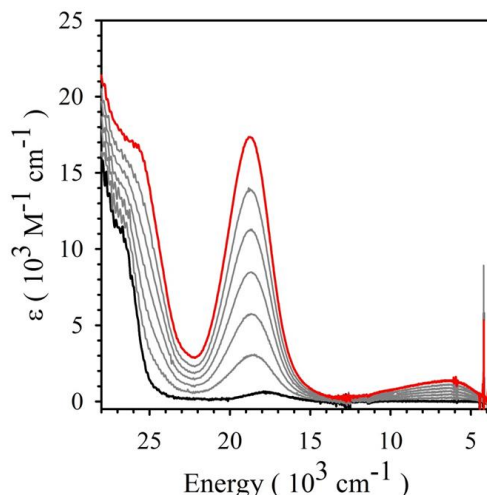


Figure 4. Electronic spectra of Cu(Sal^{CF3}) (black), [Cu(Sal^{CF3})]⁺⁺ (red) in CH₂Cl₂ at 198 K. Intermediate gray lines measured during the oxidation titration with N(C₆H₃Br₂)₃SbF₆.

3.5 Continuous wave X-band Electron Paramagnetic Resonance. The X-band EPR spectrum of [Ni(Sal^{CF3})]⁺⁺ collected at 195 K in CH₂Cl₂ showed a broad isotropic signal at $g_{\text{iso}} = 2.067$ (Figure 5a and Table 4). A minor signal at $g = 2.003$ is preliminarily assigned as an organic decomposition product, accounting for 3% of the overall signal by spin integration. Due to solvent effects, collection of this spectrum was performed in a capillary tube with a much smaller sample volume, resulting in decreased signal strength. The observed g -value suggests increased metal contribution to the SOMO when compared to other [Ni(Sal^R)]⁺⁺ complexes,^{12c} which is further corroborated with DFT calculations (*vide infra*). Upon freezing, a rhombic spectrum made up of two components with g_{av} of *ca.* 2.18 was observed (20 K), indicating the formation of two distinct Ni^{III} species (Figure 5b). This likely arises from the axial ligation of a donor species (D, most likely adventitious H₂O from sample preparation) in solution upon freezing, as the g_{av} value suggests a shift in the locus of oxidation from ligand to metal to generate a [Ni^{III}(Sal^{CF3})(D)_x]⁺ (X = 1 or 2) species. In contrast, the EPR spectrum of [Ni(Sal^{tBu})]⁺⁺ at 20 K, prepared under the same conditions, exhibits a ligand radical g -value ($g_1 = 2.063$, $g_2 = 2.013$, $g_3 = 1.988$, $g_{\text{av}} = 2.021$), indicating that [Ni(Sal^{tBu})]⁺⁺ maintains lig-

and radical character upon freezing.³⁸ As expected, the addition of 30 equivalents of pyridine and subsequent freezing results in a rhombic spectrum, which has been previously observed in the formation of $[\text{Ni}^{\text{III}}(\text{Sal}^{\text{Bu}})(\text{py})_2]^+$ (Figure 5c).^{12g} In addition, hyperfine coupling to the two nitrogen nuclei from the pyridine moieties was observed. The shift in g -value between frozen $[\text{Ni}(\text{Sal}^{\text{CF}_3})]^{2+}$ and $[\text{Ni}^{\text{III}}(\text{Sal}^{\text{Bu}})(\text{py})_2]^+$ suggests that it is sensitive to the identity of the axial ligand. This has been observed previously for a DMF adduct of $[\text{Ni}(\text{Sal}^{\text{Bu}})]^{2+}$.¹²ⁿ

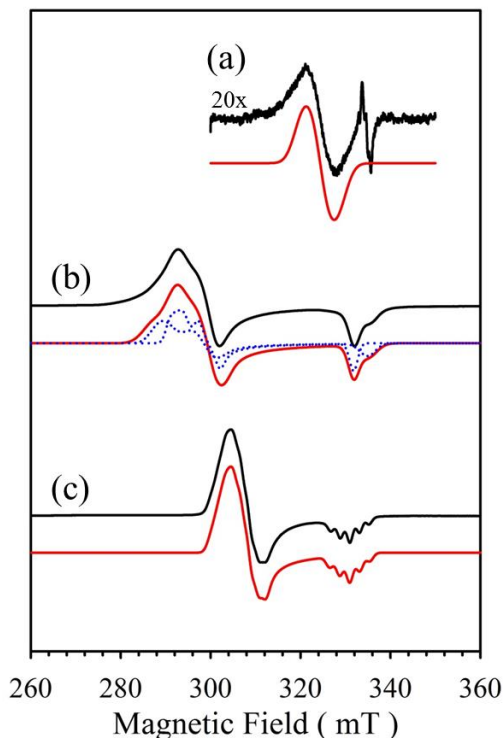


Figure 5. X-band EPR spectra for: (a) $[\text{Ni}(\text{Sal}^{\text{CF}_3})]^{2+}$ at 195 K; (b) $[\text{Ni}^{\text{III}}(\text{Sal}^{\text{CF}_3})(\text{D})_X]^+$ ($X = 1$ or 2) at 20 K and (c) $[\text{Ni}^{\text{III}}(\text{Sal}^{\text{CF}_3})(\text{py})_2]^+$ at 20 K in CH_2Cl_2 . Experimental spectrum: black, Overall simulations: red, Individual species: blue dotted. Conditions: Frequency: (a) 9.386 GHz, (b) 9.383 GHz and (c) 9.380 GHz; Power: 2.0 mW; modulation frequency: 100 kHz; amplitude 0.6 mT. See experimental section for details.

Table 4. X-band EPR simulation parameters for $[\text{Ni}(\text{Sal}^{\text{CF}_3})]^{2+}$ complexes.

Compound	g_x	g_y	g_z	g_{av}
$[\text{Ni}(\text{Sal}^{\text{CF}_3})]^{2+}$, 195 K ^a	-	-	-	2.067
$[\text{Ni}(\text{Sal}^{\text{CF}_3})]^{2+}$, 20 K, S_1 ^b	2.328	2.247	2.001	2.192
$[\text{Ni}(\text{Sal}^{\text{CF}_3})]^{2+}$, 20 K, S_2 ^b	2.291	2.234	2.020	2.182
$[\text{Ni}^{\text{III}}(\text{Sal}^{\text{CF}_3})(\text{py})_2]^+$, 20 K ^b	2.209	2.171	2.025	2.135

^a Collected in a capillary tube.

^b Collected in a 4 mm outer diameter EPR tube

S_1 = Species 1; S_2 = Species 2

The X-band EPR spectrum of $\text{Cu}(\text{Sal}^{\text{CF}_3})$ collected at 20 K exhibited features consistent with a square planar d^9 Cu^{II} center as observed for other $\text{Cu}(\text{Sal}^{\text{R}})$ complexes (Figure 6, simulation parameters: $g_{\parallel} = 2.193$, $g_{\perp} = 2.046$, $A_{\text{Cu}\parallel} = 575$, $A_{\text{Ni}\parallel} = 85$, $A_{\text{Cu}\perp} = 30$, $A_{\text{Ni}\perp} = 40$, A values in MHz).^{12q,37} Oxidation of $\text{Cu}(\text{Sal}^{\text{CF}_3})$ to $[\text{Cu}(\text{Sal}^{\text{CF}_3})]^+$ results in a substantial decrease in the EPR signal to

< 10% of the original intensity by spin integration, which supports the formation of a Cu^{III} species as suggested by the UV-Vis experiment. The weak EPR signal of $[\text{Cu}(\text{Sal}^{\text{CF}_3})]^+$ may arise from its thermal decomposition during sample preparation, or remaining unoxidized $\text{Cu}(\text{Sal}^{\text{CF}_3})$.

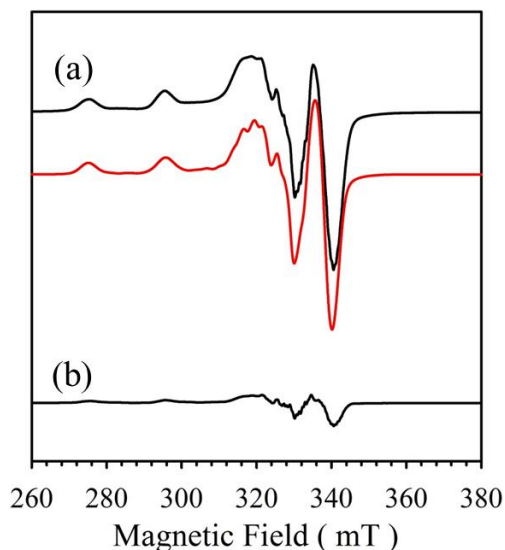


Figure 6. X-band EPR spectra for concentration matched samples of: (a) $\text{Cu}(\text{Sal}^{\text{CF}_3})$ and (b) $[\text{Cu}(\text{Sal}^{\text{CF}_3})]^+$ in CH_2Cl_2 at 20 K. Experimental spectrum: black, Simulation: red. Conditions: Frequency: (a) 9.383 GHz and (b) 9.382 GHz; Power: 2.0 mW; modulation frequency: 100 kHz; amplitude 0.6 mT.

3.6 ^{19}F NMR. Complementing the electrochemical measurements, UV-Vis-NIR and EPR data, ^{19}F NMR was used as an additional tool for evaluating the electronic structure of $\text{Ni}(\text{Sal}^{\text{CF}_3})$, $\text{Cu}(\text{Sal}^{\text{CF}_3})$ and the one-electron oxidized forms. Referenced to CFCl_3 , sharp peaks were observed for the ligand $\text{H}_2(\text{Sal}^{\text{CF}_3})$ and $\text{Ni}(\text{Sal}^{\text{CF}_3})$ at -62.8 ppm and -62.5 ppm, respectively (Figure 7a-b, Figure S6, Table 5). These chemical shifts are in agreement with other diamagnetic phenol containing compounds bearing a CF_3 moiety.^{22,43} Peak widths at half height ($W_{1/2}$) for both $\text{H}_2(\text{Sal}^{\text{CF}_3})$ and $\text{Ni}(\text{Sal}^{\text{CF}_3})$ were 3 Hz, as expected for a diamagnetic compound (Table 5). On the other hand, $\text{Cu}(\text{Sal}^{\text{CF}_3})$ exhibited a broad signal at -64.4 ppm with $W_{1/2} = 135$ Hz due to the paramagnetic Cu^{II} center (Figure 7c). The ^{19}F peak for $\text{Ni}(\text{Sal}^{\text{CF}_3})$ disappears upon oxidation to $[\text{Ni}(\text{Sal}^{\text{CF}_3})]^{2+}$, consistent with the formation of a ligand radical in close proximity to the CF_3 moieties (Figure S7). In contrast, loss of the broad ^{19}F signal of $\text{Cu}(\text{Sal}^{\text{CF}_3})$ was accompanied by the appearance of two signals upon oxidation to $[\text{Cu}(\text{Sal}^{\text{CF}_3})]^+$: (Figure 7d). A major signal at -63.2 ppm ($W_{1/2} = 35$ Hz) and minor signal at -64.0 ppm ($W_{1/2} = 3$ Hz). The minor signal is attributed to a decomposition product from the oxidation reaction, and increases over time (Table 5, Figure S9).

Table 5. ^{19}F NMR chemical shifts.

Compound	Chemical Shift (ppm) ^a	$W_{1/2}$ (Hz)
$\text{H}_2(\text{Sal}^{\text{CF}_3})$	-62.8	3
$\text{Ni}(\text{Sal}^{\text{CF}_3})$	-62.5	3
$[\text{Ni}(\text{Sal}^{\text{CF}_3})]^{2+}$	-	-
$\text{Cu}(\text{Sal}^{\text{CF}_3})$	-64.4	135
$[\text{Cu}(\text{Sal}^{\text{CF}_3})]^+$	-63.2	35
	-64.0	3

^a Chemical shift relative to CFCl_3 .

The decomposition is consistent with the limited stability of $[\text{Cu}(\text{Sal}^{\text{CF}_3})]^+$ in solution ($t_{1/2} = 150$ minutes at 298 K). The relatively sharp ^{19}F peak for $[\text{Cu}(\text{Sal}^{\text{CF}_3})]^+$ is assigned to a Cu^{III} species (Figure 7d), the broadness in the signal is likely due to fast electron exchange with a paramagnetic decomposition product. It should be noted that the signal for the SbF_6^- counterion could not be detected due to the quadrupolar moment of the Sb center.⁴⁴

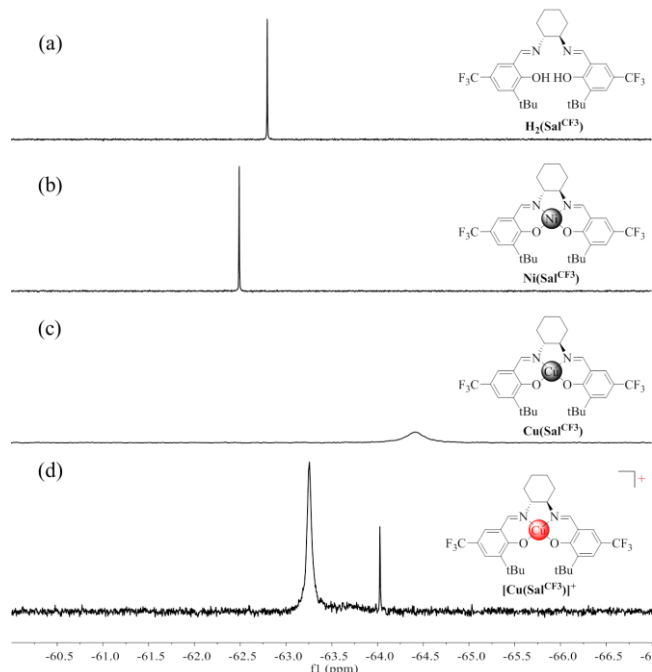


Figure 7. ^{19}F NMR spectra of (a) $\text{H}_2(\text{Sal}^{\text{CF}_3})$; (b) $\text{Ni}(\text{Sal}^{\text{CF}_3})$, (c) $\text{Cu}(\text{Sal}^{\text{CF}_3})$ and (d) $[\text{Cu}(\text{Sal}^{\text{CF}_3})]^+$ recorded in CH_2Cl_2 at 298 K.

3.7 X-ray Photoelectron Spectroscopy (XPS). Ni and Cu XPS was used to evaluate the metal oxidation states in both the neutral and oxidized complexes in the solid state. Referenced to the C 1s binding energy, the metal $2p_{3/2}$ and $2p_{1/2}$ binding energies (Table 6) for both neutral complexes indicate a common 2+ oxidation state, as previously observed for structurally similar Ni^{45} and Cu^{12f} complexes. Upon oxidation, the Ni $2p_{3/2}$ and $2p_{1/2}$ binding energies for $[\text{Ni}(\text{Sal}^{\text{CF}_3})]^{++}$ experience a small shift towards higher energies (Figure S10 and Table 6), supporting the formation of a Ni^{II} -phenoxyl rather than a Ni^{III} -phenolate species in the solid state. Fluorine *KLL* peaks (Auger transition) at 856.8 eV and 876.2 eV are also visible in both the oxidized Ni and Cu complexes (Figure S11).⁴⁶ On the other hand, a larger shift in binding energy (*ca.* 1.8 eV, Figure S12) was observed from oxidation of $\text{Cu}(\text{Sal}^{\text{CF}_3})$ to $[\text{Cu}(\text{Sal}^{\text{CF}_3})]^+$. This indicates a change in Cu oxidation state from 2+ to 3+, consistent with a previous report on $[\text{Cu}(\text{Sal}^{\text{tBu}})]^+$, which showed a shift in binding energy of *ca.* 1.8 eV in comparison to its neutral form.

Table 6. Metal (2p) binding energies vs. C(1s) (284.8 eV).

Compound	Binding Energy (eV)	
	$2p_{3/2}$	$2p_{1/2}$
$\text{Ni}(\text{Sal}^{\text{CF}_3})$	872.1	854.8
$[\text{Ni}(\text{Sal}^{\text{CF}_3})]^{++}$	872.1	854.9
$\text{Cu}(\text{Sal}^{\text{CF}_3})$	954.0	934.1
$[\text{Cu}(\text{Sal}^{\text{CF}_3})]^+$	955.9	935.9

3.8 Theoretical analysis. **3.8.1. $\text{Ni}(\text{Sal}^{\text{CF}_3})$.** A symmetric structure was predicted for $\text{Ni}(\text{Sal}^{\text{CF}_3})$ using the B3LYP function-

al with a polarized continuum model (PCM) for CH_2Cl_2 (Table S1). A symmetric structure was also predicted for $[\text{Ni}(\text{Sal}^{\text{CF}_3})]^{++}$, with a contraction in the coordination sphere in comparison to $\text{Ni}(\text{Sal}^{\text{CF}_3})$ (Table S1). A delocalized electronic structure, in which the ligand radical is distributed over both aromatic phenolates, was predicted for $[\text{Ni}(\text{Sal}^{\text{CF}_3})]^{++}$ (Figure 8), in agreement with the sharp and intense NIR bands observed in the UV-Vis-NIR spectrum (Figure 3). The predicted spin density on the nickel center for $[\text{Ni}(\text{Sal}^{\text{CF}_3})]^{++}$ (SD_{Ni} : 34%), and thus metal contribution to the SOMO is higher in comparison to other $[\text{Ni}(\text{Sal}^{\text{R}})]^{++}$ complexes ($[\text{Ni}(\text{Sal}^{\text{tBu}})]^{++}$: SD_{Ni} : 22%; $[\text{Ni}(\text{Sal}^{\text{OMe}})]^{++}$: SD_{Ni} : 12%; $[\text{Ni}(\text{Sal}^{\text{NMe}_2})]^{++}$: SD_{Ni} : 5%). This observation follows the trends established previously for other $[\text{Ni}(\text{Sal}^{\text{R}})]^{++}$ complexes, where electron-donating *para*-ring substituents decrease the metal contribution to the SOMO,^{12c,47} and is in agreement with the increased *g*-value in the EPR spectrum of $[\text{Ni}(\text{Sal}^{\text{CF}_3})]^{++}$ (Figure 5). Using CAM-B3LYP as the functional with no solvent model also predicted a symmetric structure for $[\text{Ni}(\text{Sal}^{\text{CF}_3})]^{++}$, albeit with slightly different SD_{Ni} values.⁴⁷

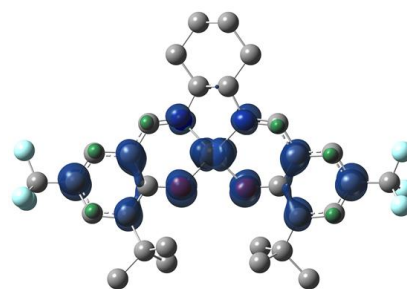
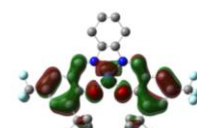
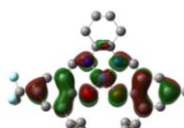


Figure 8. Spin density plot of $[\text{Ni}(\text{Sal}^{\text{CF}_3})]^{++}$ ($\text{SD}_{\text{Ni}} = 34\%$). See experimental section for calculation details.

Time-Dependent Density Functional Theory (DFT) calculations³³ were undertaken to gain insight into the spectral features of $[\text{Ni}(\text{Sal}^{\text{CF}_3})]^{++}$. Two NIR transitions were predicted for $[\text{Ni}(\text{Sal}^{\text{CF}_3})]^{++}$ (Figure 3), and the natural transition orbitals (NTOs)⁴⁸ contributing to the transitions are shown in Table 7.

The lowest energy transition predicted at 5700 cm^{-1} matches well with the experimental energy, and is predicted to be a delocalized intra-ligand charge transfer (ILCT) transition, with donation to the imine nitrogens. The higher energy band (9300 cm^{-1}) is predicted to be more intense and the NTOs involved are fully delocalized over the ligand framework (Table 7). Such intense NIR transitions have also been predicted for the similarly delocalized species $[\text{Ni}(\text{Sal}^{\text{tBu}})]^{++}$ (Table S2).^{12c} These calculations support the experimental data obtained in these studies in the assignment of $[\text{Ni}(\text{Sal}^{\text{CF}_3})]^{++}$ as a Class III intervalence compound.

Table 7. Natural Transition Orbitals (NTO) representing the transitions contributing to the two NIR bands of $[\text{Ni}(\text{Sal}^{\text{CF}_3})]^{++}$. See experimental section for calculation details.

Excited State Properties	Holes	Electrons
<u>Excited State 1</u>		
$\nu_{\text{calc}} = 5700\text{ cm}^{-1}$		
$f = 0.0717$		
$\nu_{\text{exp}} = 4900\text{ cm}^{-1}$		
$\epsilon = 16200\text{ M}^{-1}\text{ cm}^{-1}$		

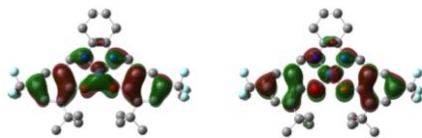
Excited State 3

$$\nu_{\text{calc}} = 9300 \text{ cm}^{-1}$$

$$f = 0.1248$$

$$\nu_{\text{exp}} = 8600 \text{ cm}^{-1}$$

$$\epsilon = 13100 \text{ M}^{-1} \text{ cm}^{-1}$$



3.8.2. **Cu(Sal^{CF3})**. A symmetric structure was predicted for **Cu(Sal^{CF3})** within $\pm 0.01 \text{ \AA}$ of the experimental values using the B3LYP functional with a polarized continuum model (PCM) for CH_2Cl_2 (Table S1). The predicted spin density of **Cu(Sal^{CF3})** shows spin-covalency between the Cu $d_{x^2-y^2}$ orbital and the coordinating atoms, as expected for a d^9 metal complex (Figure S12).

Oxidation of **Cu(Sal^{CF3})** can afford one of three electronic states: (i) a d^8 Cu^{III} -salen complex ($S = 0$), (ii) a Cu^{II} complex antiferromagnetically coupled to a phenoxyl radical (broken symmetry, $S = 0$), or (iii) a Cu^{II} complex ferromagnetically coupled to a phenoxyl radical ($S = 1$). All three possibilities were explored, where the broken symmetry solution converges to the singlet solution, which has been previously observed for calculations of **[Cu(Sal^{IBu})]⁺** using the same level of theory.^{12f} The $S = 0$ solution for **[Cu(Sal^{CF3})]⁺** was predicted to be lowest in energy by 3.3 kcal/mol, which is in agreement with the experimental data. This is consistent with **[Cu(Sal^{CF3})]⁺** being a Cu^{III} -salen species, in comparison to **[Cu(Sal^{IBu})]⁺** where an equilibrium between Cu^{III} -salen and a Cu^{II} -phenoxyl radical species was observed.

4. Discussion and Summary

Chemical oxidation of **Ni(Sal^{CF3})** monitored by UV-Vis-NIR showed the formation of a delocalized ligand radical species, evidenced by the appearance of sharp and intense NIR transitions (Figure 3). This is supported by a negligible shift in metal binding energy by XPS as well as the disappearance of the ^{19}F NMR spectrum upon oxidation. An isotropic signal ($g = 2.067$) indicative of a ligand radical was observed in the solution state EPR of **[Ni(Sal^{CF3})]²⁺**, and this g -value is higher in comparison to other **[Ni(Sal^R)]²⁺**, consistent with an increase in metal character for the SOMO of **[Ni(Sal^{CF3})]²⁺** due to the electron withdrawing CF_3 substituents (Figure 5a). Interestingly, a rhombic signal comprised of two species at $g_{\text{av}} \sim 2.18$ was observed upon freezing, signifying the formation of a Ni^{III} species (Figure 5b). Typically, a low spin $S = 1/2$ Ni^{III} center will display such a rhombic EPR pattern with g_{av} values *ca.* 2.12 – 2.17.^{16,18,49} The EPR spectrum of **[Ni(Sal^{CF3})]²⁺** exhibits two similar g_{\parallel} (g_x and g_y) and g_{\perp} (g_z) features, a pattern that is consistent with previous reports of 5 or 6 coordinate Ni^{III} species.^{16,18,49-50} This is in contrast to 4-coordinate Ni^{III} species, where a single g_{\parallel} and two similar g_{\perp} components are observed.¹⁶ This suggests the shift in oxidation locus of **[Ni(Sal^{CF3})]²⁺** upon freezing is due to adventitious axial ligand binding, a process that is favored in comparison to **[Ni(Sal^{IBu})]²⁺**, as a result of increased Lewis acidity of the Ni center.

Time-dependent DFT calculations further support a delocalized electronic structure, correctly predicting the two intense NIR electronic transitions for **[Ni(Sal^{CF3})]²⁺**. Interestingly, the two low energy bands display a similar intensity (Figure 3), while for **[Ni(Sal^{IBu})]²⁺** (Figure S15) the lowest energy transition is 3-fold more intense. To gain further insight into this difference we analyzed the TD-DFT transitions employing natural transition orbitals (NTO).⁴⁸ While the calculated oscillator strengths do not correctly predict the experimental ratio observed for **[Ni(Sal^{CF3})]²⁺**, the change in predicted orbital intensities in comparison to **[Ni(Sal^{IBu})]²⁺** (Figure S15) offers insight into the nature of the

electronic transitions for these two ligand radical complexes. For **[Ni(Sal^{CF3})]²⁺**, the low energy transition is predicted to have significant ILCT character with donation to the imine nitrogens (Table 7), while the NTOs for the higher energy transition are fully delocalized, and the increased intensity reflects greater overlap between the donor and acceptor orbitals.⁵¹ For **[Ni(Sal^{IBu})]²⁺**, the higher energy transition is predicted to have significant donation to the phenolate oxygens (Table S2), while the NTOs for the lowest energy transition are fully delocalized with significant overlap between the donor and acceptor orbitals. This data suggests that the *para*-ring electron-withdrawing group not only serves to increase the charge density on the Ni center, but also alters the nature of the low energy ligand radical electronic transitions.

Upon oxidation, **[Cu(Sal^{CF3})]⁺** demonstrates the characteristics of a diamagnetic species, with a significant decrease in the EPR signal (Figure 6) as well as the sharpening of the ^{19}F NMR signal (Figure 7). This was further evidenced by the appearance of an intense transition at *ca.* $18000 \text{ M}^{-1} \text{ cm}^{-1}$ in the UV-Vis-NIR spectra, a characteristic LMCT for a Cu^{III} -salen complex, suggesting the locus of oxidation for **[Cu(Sal^{CF3})]⁺** is primarily metal-based. XPS measurements further support **[Cu(Sal^{CF3})]⁺** as a Cu^{III} species in the solid state, where the binding energy of the metal center is shifted upwards of 1.8 eV upon oxidation from its neutral counterpart. Interestingly, **[Cu(Sal^{IBu})]⁺** exists in a reversible temperature-dependent equilibrium in solution between a Cu^{III} -phenolate and a Cu^{II} -phenoxyl species, which is manifested in a reduction of its LMCT band by *ca.* 50% upon an increase in temperature.^{12f} This equilibrium could not be probed fully for **[Cu(Sal^{CF3})]⁺** due to its thermal instability above 233 K ($t_{1/2} = 150$ minutes at 298 K, Figure S5). However, spectra at 198 K and 233 K do not show appreciable differences (Figure S5), suggesting that in this temperature range the Cu^{III} -phenolate electronic state is stabilized. The significant decrease in the electronic spectra at 273 K is attributed to decomposition. In addition, the calculated electronic energies support the formation of a Cu^{III} -phenolate species, where this electronic state is favored over a triplet Cu^{II} -phenoxyl radical species by 3.3 kcal/mol. Under the same calculation parameters, the $S = 1$ Cu^{II} -phenoxyl radical solution for **[Cu(Sal^{IBu})]⁺** is favored by 1.3 kcal/mol,^{12f} further supporting that **[Cu(Sal^{CF3})]⁺** exhibits greater Cu^{III} character in comparison to **[Cu(Sal^{IBu})]⁺**. Overall, these results show that Ni and Cu complexes of the electron-poor salen ligand **H₂Sal^{CF3}** afford a delocalized phenoxyl radical complex for Ni, and a high-valent metal complex in the case of Cu.

ASSOCIATED CONTENT

Supporting Information

Full reference for 28, cif file of **Cu(Sal^{CF3})**, Hammett analysis of oxidative potentials of **Ni(Sal^R)**, pyridine binding titrations for **Ni(Sal^{CF3})**, VT UV-Vis-NIR spectra of **[Cu(Sal^{CF3})]⁺**, additional ^{19}F NMR plots and further computational data are compiled in the supporting information. This material is available free of charge via the Internet at <http://pubs.acs.org>.

AUTHOR INFORMATION

Corresponding Author

*Email: tim_storr@sfu.ca

ACKNOWLEDGMENT

This work is supported by a NSERC Discovery Grant (T.S.), and a travel grant from the France-Canada Research Fund (T.S. and F.T.). L.C. thanks NSERC for a Research Exchange Travel Award. Compute Canada and Westgrid are acknowledged for access to computational resources.

REFERENCES

- (a) Lyons, C. T.; Stack, T. D. P., *Coord. Chem. Rev.*, **2013**, *257*, 528-540; (b) Luca, O. R.; Crabtree, R. H., *Chem. Soc. Rev.*, **2013**, *42*, 1440-1459; (c) de Bruin, B., *Eur. J. Inorg. Chem.*, **2012**, 340-342; (d) Lyaskovskyy, V.; de Bruin, B., *ACS Catal.*, **2012**, *2*, 270-279; (e) Kaim, W., *Eur. J. Inorg. Chem.*, **2012**, 343-348; (f) Chirik, P. J., *Inorg. Chem.*, **2011**, *50*, 9737-9740.
- (a) Whittaker, J. W., *Chem. Rev.*, **2003**, *103*, 2347-2363; (b) Thomas, F., *Stable Radicals: Fundamentals and Applied Aspects of Odd-Electron Compounds*. 2010; p 1-588.
- Rittle, J.; Green, M. T., *Science*, **2010**, *330*, 933-937.
- (a) Hendrickson, D. N.; Pierpont, C. G., Valence tautomeric transition metal complexes. In *Spin Crossover in Transition Metal Compounds II*, Springer: 2004; Vol. 234, pp 63-95; (b) Pierpont, C. G., *Coord. Chem. Rev.*, **2001**, *219*, 415-433; (c) Pierpont, C. G., *Coord. Chem. Rev.*, **2001**, *216*, 99-125; (d) Pierpont, C. G.; Lange, C. W., The chemistry of transition-metal complexes containing catechol and semiquinone ligands. In *Prog. Inorg. Chem.*, Karlin, K. D., Ed. 1994; Vol. 41, pp 331-442.
- (a) Ray, K.; George, S. D.; Solomon, E. I.; Wiegardt, K.; Neese, F., *Chem. Eur. J.*, **2007**, *13*, 2783-2797; (b) Ray, K.; Weyhermuller, T.; Neese, F.; Wiegardt, K., *Inorg. Chem.*, **2005**, *44*, 5345-5360.
- (a) Chaudhuri, P.; Wiegardt, K., Phenoxyl radical complexes. In *Prog. Inorg. Chem.*, 2001; Vol. 50, pp 151-216; (b) Allard, M. M.; Sonk, J. A.; Heeg, M. J.; McGarvey, B. R.; Schlegel, H. B.; Verani, C. N., *Angew. Chem. Int. Ed.*, **2012**, *51*, 3178-3182.
- (a) Bachler, V.; Olbrich, G.; Neese, F.; Wiegardt, K., *Inorg. Chem.*, **2002**, *41*, 4179-4193; (b) Herebian, D.; Bothe, E.; Bill, E.; Weyhermuller, T.; Wiegardt, K., *J. Am. Chem. Soc.*, **2001**, *123*, 10012-10023; (c) Mederos, A.; Dominguez, S.; Hernandez-Molina, R.; Sanchiz, J.; Brito, F., *Coord. Chem. Rev.*, **1999**, *193-5*, 857-911; (d) Peng, S. M.; Chen, C. T.; Liaw, D. S.; Chen, C. I.; Yu, W., *Inorg. Chim. Acta*, **1985**, *101*, L31-L33.
- (a) Bill, E.; Bothe, E.; Chaudhuri, P.; Chlopek, K.; Herebian, D.; Kokatam, S.; Ray, K.; Weyhermuller, T.; Neese, F.; Wiegardt, K., *Chem. Eur. J.*, **2004**, *11*, 204-224; (b) Blackmore, K. J.; Sly, M. B.; Haneline, M. R.; Ziller, J. W.; Heyduk, A. F., *Inorg. Chem.*, **2008**, *47*, 10522-10532; (c) Smith, A. L.; Hardcastle, K. I.; Soper, J. D., *J. Am. Chem. Soc.*, **2010**, *132*, 14358-14360; (d) Rajput, A.; Sharma, A. K.; Barman, S. K.; Koley, D.; Steinert, M.; Mukherjee, R., *Inorg. Chem.*, **2014**, *53*, 36-48; (e) Das, D.; Agarwala, H.; Chowdhury, A. D.; Patra, T.; Mobin, S. M.; Sarkar, B.; Kaim, W.; Lahiri, G. K., *Chem. Eur. J.*, **2013**, *19*, 7384-7394; (f) Das, D.; Scherer, T. M.; Das, A.; Mondal, T. K.; Mobin, S. M.; Fiedler, J.; Luis Priego, J.; Jimenez-Aparicio, R.; Kaim, W.; Lahiri, G. K., *Dalton Trans.*, **2012**, *41*, 11675-11683; (g) Huebner, R.; Sarkar, B.; Fiedler, J.; Zalis, S.; Kaim, W., *Eur. J. Inorg. Chem.*, **2012**, 3569-3576.
- (a) Bart, S. C.; Chlopek, K.; Bill, E.; Bouwkamp, M. W.; Lobkovsky, E.; Neese, F.; Wiegardt, K.; Chirik, P. J., *J. Am. Chem. Soc.*, **2006**, *128*, 13901-13912; (b) Bowman, A. C.; Sproules, S.; Wiegardt, K., *Inorg. Chem.*, **2012**, *51*, 3707-3717; (c) de Bruin, B.; Bill, E.; Bothe, E.; Weyhermuller, T.; Wiegardt, K., *Inorg. Chem.*, **2000**, *39*, 2936-2947; (d) England, J.; Scarborough, C. C.; Weyhermuller, T.; Sproules, S.; Wiegardt, K., *Eur. J. Inorg. Chem.*, **2012**, 4605-4621; (e) Lu, C. C.; Bill, E.; Weyhermuller, T.; Bothe, E.; Wiegardt, K., *J. Am. Chem. Soc.*, **2008**, *130*, 3181-3197; (f) Lu, C. C.; George, S. D.; Weyhermuller, T.; Bill, E.; Bothe, E.; Wiegardt, K., *Angew. Chem. Int. Ed.*, **2008**, *47*, 6384-6387; (g) Lu, C. C.; Weyhermuller, T.; Bill, E.; Wiegardt, K., *Inorg. Chem.*, **2009**, *48*, 6055-6064; (h) Scarborough, C. C.; Sproules, S.; Weyhermuller, T.; DeBeer, S.; Wiegardt, K., *Inorg. Chem.*, **2011**, *50*, 12446-12462; (i) Tondreau, A. M.; Milsmann, C.; Patrick, A. D.; Hoyt, H. M.; Lobkovsky, E.; Wiegardt, K.; Chirik, P. J., *J. Am. Chem. Soc.*, **2010**, *132*, 15046-15059; (j) Wang, M.; England, J.; Weyhermuller, T.; Wiegardt, K., *Inorg. Chem.*, **2014**, *53*, 2276-2287; (k) Wang, M.; Weyhermuller, T.; England, J.; Wiegardt, K., *Inorg. Chem.*, **2013**, *52*, 12763-12776.
- (a) Adhikari, D.; Mossin, S.; Basuli, F.; Huffman, J. C.; Szilagy, R. K.; Meyer, K.; Mindiola, D. J., *J. Am. Chem. Soc.*, **2008**, *130*, 3676-3682; (b) Aienza, C. C. H.; Bowman, A. C.; Lobkovsky, E.; Chirik, P. J., *J. Am. Chem. Soc.*, **2010**, *132*, 16343-16345; (c) Buttner, T.; Geier, J.; Frison, G.; Harmer, J.; Calle, C.; Schweiger, A.; Schonberg, H.; Grutzmacher, H., *Science*, **2005**, *307*, 235-238; (d) Haneline, M. R.; Heyduk, A. F., *J. Am. Chem. Soc.*, **2006**, *128*, 8410-8411; (e) Koenigsmann, M.; Donati, N.; Stein, D.; Schoenberg, H.; Harmer, J.; Sreekanth, A.; Gruetzmacher, H., *Angew. Chem. Int. Ed.*, **2007**, *46*, 3567-3570; (f) Maire, P.; Konigsmann, M.; Sreekanth, A.; Harmer, J.; Schweiger, A.; Grutzmacher, H., *J. Am. Chem. Soc.*, **2006**, *128*, 6578-6580; (g) Miyazato, Y.; Wada, T.; Tanaka, K., *Bull. Chem. Soc. Jpn.*, **2006**, *79*, 745-747; (h) Ringenberg, M. R.; Kokatam, S. L.; Heiden, Z. M.; Rauchfuss, T. B., *J. Am. Chem. Soc.*, **2008**, *130*, 788-788; (i) Zarkesh, R. A.; Ziller, J. W.; Heyduk, A. F., *Angew. Chem. Int. Ed.*, **2008**, *47*, 4715-4718.
- (a) Dolphin, D.; Niemi, T.; Felton, R. H.; Fujita, I., *J. Am. Chem. Soc.*, **1975**, *97*, 5288-5290; (b) Ohtsu, H.; Tanaka, K., *Angew. Chem. Int. Ed.*, **2004**, *43*, 6301-6303; (c) Puschmann, F. F.; Harmer, J.; Stein, D.; Rueeeger, H.; de Bruin, B.; Gruetzmacher, H., *Angew. Chem. Int. Ed.*, **2010**, *49*, 385-389.
- (a) de Bellefeuille, D.; Askari, M. S.; Lassalle-Kaiser, B.; Journaux, Y.; Aukauloo, A.; Orio, M.; Thomas, F.; Ottenwaelder, X., *Inorg. Chem.*, **2012**, *51*, 12796-12804; (b) Asami, K.; Tsukidate, K.; Iwatsuki, S.; Tani, F.; Karasawa, S.; Chiang, L.; Storr, T.; Thomas, F.; Shimazaki, Y., *Inorg. Chem.*, **2012**, *51*, 12450-12461; (c) Chiang, L.; Kochem, A.; Jarjayes, O.; Dunn, T. J.; Vezin, H.; Sakaguchi, M.; Ogura, T.; Orio, M.; Shimazaki, Y.; Thomas, F.; Storr, T., *Chem. Eur. J.*, **2012**, *18*, 14117-14127; (d) Shimazaki, Y.; Arai, N.; Dunn, T. J.; Yajima, T.; Tani, F.; Ramogida, C. F.; Storr, T., *Dalton Trans.*, **2011**, *40*, 2469-2479; (e) Shimazaki, Y.; Stack, T. D. P.; Storr, T., *Inorg. Chem.*, **2009**, *48*, 8383-8392; (f) Storr, T.; Verma, P.; Pratt, R. C.; Wasinger, E. C.; Shimazaki, Y.; Stack, T. D. P., *J. Am. Chem. Soc.*, **2008**, *130*, 15448-15459; (g) Storr, T.; Wasinger, E. C.; Pratt, R. C.; Stack, T. D. P., *Angew. Chem. Int. Ed.*, **2007**, *46*, 5198-5201; (h) Rotthaus, O.; Jarjayes, O.; Del Valle, C. P.; Philouze, C.; Thomas, F., *Chem. Commun.*, **2007**, 4462-4464; (i) Rotthaus, O.; Jarjayes, O.; Philouze, C.; Del Valle, C. P.; Thomas, F., *Dalton Trans.*, **2009**, 1792-1800; (j) Rotthaus, O.; Jarjayes, O.; Thomas, F.; Philouze, C.; Del Valle, C. P.; Saint-Aman, E.; Pierre, J. L., *Chem. Eur. J.*, **2006**, *12*, 2293-2302; (k) Rotthaus, O.; Thomas, F.; Jarjayes, O.; Philouze, C.; Saint-Aman, E.; Pierre, J.-L., *Chem. Eur. J.*, **2006**, *12*, 6953-6962; (l) Kochem, A.; Jarjayes, O.; Baptiste, B.; Philouze, C.; Vezin, H.; Tsukidate, K.; Tani, F.; Orio, M.; Shimazaki, Y.; Thomas, F., *Chem. Eur. J.*, **2012**, *18*, 1068-1072; (m) Kochem, A.; Kanso, H.; Baptiste, B.; Arora, H.; Philouze, C.; Jarjayes, O.; Vezin, H.; Luneau, D.; Orio, M.; Thomas, F., *Inorg. Chem.*, **2012**, *51*, 10557-10571; (n) Shimazaki, Y.; Tani, F.; Fukui, K.; Naruta, Y.; Yamauchi, O., *J. Am. Chem. Soc.*, **2003**, *125*, 10512-10513; (o) Pratt, R. C.; Lyons, C. T.; Wasinger, E. C.; Stack, T. D. P., *J. Am. Chem. Soc.*, **2012**, *134*, 7367-7377; (p) Verma, P.; Pratt, R. C.; Storr, T.; Wasinger, E. C.; Stack, T. D. P., *Proc. Natl. Acad. Sci. U.S.A.*, **2011**, *108*, 18600-18605; (q) Orio, M.; Jarjayes, O.; Kanso, H.; Philouze, C.; Neese, F.; Thomas, F., *Angew. Chem. Int. Ed.*, **2010**, *49*, 4989-4992; (r) Orio, M.; Philouze, C.; Jarjayes, O.; Neese, F.; Thomas, F., *Inorg. Chem.*, **2010**, *49*, 646-658; (s) Kurahashi, T.; Fujii, H., *Inorg. Chem.*, **2013**, *52*, 3908-3919; (t) Kurahashi, T.; Fujii, H., *Bull. Chem. Soc. Jpn.*, **2012**, *85*, 940-947; (u) Kurahashi, T.; Fujii, H., *J. Am. Chem. Soc.*, **2011**, *133*, 8307-8316; (v) Wang, C.; Kurahashi, T.; Fujii, H., *Angew. Chem. Int. Ed.*, **2012**, *51*, 7809-7811.
- (a) Canali, L.; Sherrington, D. C., *Chem. Soc. Rev.*, **1999**, *28*, 85-93; (b) Darenbourg, D. J., *Chem. Rev.*, **2007**, *107*, 2388-2410; (c) Irie, R.; Noda, K.; Ito, Y.; Matsumoto, N.; Katsuki, T., *Tetrahedron Lett.*, **1990**, *31*, 7345-7348; (d) Jacobsen, E. N.; Zhang, W.; Muci, A. R.; Ecker, J. R.; Deng, L., *J. Am. Chem. Soc.*, **1991**, *113*, 7063-7064; (e) McGarrigle, E. M.; Gilheany, D. G., *Chem. Rev.*, **2005**, *105*, 1563-1602.
- Dunn, T. J.; Chiang, L.; Ramogida, C. F.; Hazin, K.; Webb, M. I.; Katz, M. J.; Storr, T., *Chem. Eur. J.*, **2013**, *19*, 9606-9618.
- (a) Kochem, A.; Gellon, G.; Jarjayes, O.; Philouze, C.; Leconte, N.; van Gastel, M.; Bill, E.; Thomas, F., *Chem. Commun.*, **2014**, *50*, 4924-4926; (b) Kochem, A.; Thomas, F.; Jarjayes, O.; Gellon, G.; Philouze, C.; Weyhermuller, T.; Neese, F.; van Gastel, M., *Inorg. Chem.*, **2013**, *52*, 14428-14438; (c) Carrasco, R.; Cano, J.; Ottenwaelder, X.; Aukauloo, A.; Journaux, Y.; Ruiz-Garcia, R., *Dalton Trans.*, **2005**, 2527-2538; (d) Cohen, C. T.; Thomas, C. M.; Peretti, K. L.; Lobkovsky, E. B.; Coates, G. W., *Dalton Trans.*, **2006**, 237-249; (e) Kemper, S.; Hrobarik, P.; Kaupp, M.; Schloerer, N. E., *J. Am. Chem. Soc.*, **2009**, *131*, 4172-4172; (f) Vinck, E.; Murphy, D. M.; Fallis, I. A.; Strevens, R. R.; Van Doorslaer, S., *Inorg. Chem.*, **2010**, *49*, 2083-2092.
- Eckshtain-Levi, M.; Orio, M.; Lavi, R.; Benisvy, L., *Dalton Trans.*, **2013**, *42*, 13323-13326.
- (a) Ottenwaelder, X.; Aukauloo, A.; Journaux, Y.; Carrasco, R.; Cano, J.; Cervera, B.; Castro, I.; Curreli, S.; Munoz, M. C.; Rosello, A. L.; Soto, B.; Ruiz-Garcia, R., *Dalton Trans.*, **2005**, 2516-2526; (b) Ottenwaelder, X.; Ruiz-Garcia, R.; Blondin, G.; Carasco, R.; Cano, J.; Lexa, D.; Journaux, Y.; Aukauloo, A., *Chem. Commun.*, **2004**, 504-505.
- Jacobs, S. A.; Margerum, D. W., *Inorg. Chem.*, **1984**, *23*, 1195-1201.
- (a) Bertz, S. H.; Cope, S.; Dorton, D.; Murphy, M.; Ogle, C. A., *Angew. Chem. Int. Ed.*, **2007**, *46*, 7082-7085; (b) Bertz, S. H.; Cope, S.; Murphy, M.; Ogle, C. A.; Taylor, B. J., *J. Am. Chem. Soc.*, **2007**, *129*,

- 7208-7208; (c) Hickman, A. J.; Sanford, M. S., *Nature*, **2012**, *484*, 177-185; (d) Hu, H.; Snyder, J. P., *J. Am. Chem. Soc.*, **2007**, *129*, 7210-7210; (e) Huffman, L. M.; Stahl, S. S., *J. Am. Chem. Soc.*, **2008**, *130*, 9196-9196; (f) Ribas, X.; Jackson, D. A.; Donnadiou, B.; Mahia, J.; Parella, T.; Xifra, R.; Hedman, B.; Hodgson, K. O.; Llobet, A.; Stack, T. D. P., *Angew. Chem. Int. Ed.*, **2002**, *41*, 2991-2994.
20. (a) Citek, C.; Lin, B.-L.; Phelps, T. E.; Wasinger, E. C.; Stack, T. D. P., *J. Am. Chem. Soc.*, **2014**, *136*, 14405-14408; (b) Cole, A. P.; Mahadevan, V.; Mirica, L. M.; Ottenwaelder, X.; Stack, T. D. P., *Inorg. Chem.*, **2005**, *44*, 7345-7364; (c) DuBois, J. L.; Mukherjee, P.; Collier, A. M.; Mayer, J. M.; Solomon, E. I.; Hedman, B.; Stack, T. D. P.; Hodgson, K. O., *J. Am. Chem. Soc.*, **1997**, *119*, 8578-8579; (d) DuBois, J. L.; Mukherjee, P.; Stack, T. D. P.; Hedman, B.; Solomon, E. I.; Hodgson, K. O., *J. Am. Chem. Soc.*, **2000**, *122*, 5775-5787; (e) Henson, M. J.; Mukherjee, P.; Root, D. E.; Stack, T. D. P.; Solomon, E. I., *J. Am. Chem. Soc.*, **1999**, *121*, 10332-10345; (f) Mahadevan, V.; DuBois, J. L.; Hedman, B.; Hodgson, K. O.; Stack, T. D. P., *J. Am. Chem. Soc.*, **1999**, *121*, 5583-5584; (g) Root, D. E.; Henson, M. J.; Machonkin, T.; Mukherjee, P.; Stack, T. D. P.; Solomon, E. I., *J. Am. Chem. Soc.*, **1998**, *120*, 4982-4990; (h) Itoh, S.; Taki, M.; Nakao, H.; Holland, P. L.; Tolman, W. B.; Que, L.; Fukuzumi, S., *Angew. Chem. Int. Ed.*, **2000**, *39*, 398-398; (i) Mahapatra, S.; Halfen, J. A.; Wilkinson, E. C.; Pan, G. F.; Cramer, C. J.; Que, L.; Tolman, W. B., *J. Am. Chem. Soc.*, **1995**, *117*, 8865-8866; (j) Mahapatra, S.; Young, V. G.; Kaderli, S.; Zuberbuhler, A. D.; Tolman, W. B., *Angew. Chem. Int. Ed.*, **1997**, *36*, 130-133.
21. Perrin, D. D.; Armarego, W. L. F., *Purification of Laboratory Chemicals*. 1st ed. ed.; Pergamo Press: New York, 1988.
22. Michel, F.; Hamman, S.; Philouze, C.; Del Valle, C. P.; Saint-Aman, E.; Thomas, F., *Dalton Trans.*, **2009**, 832-842.
23. (a) Connelly, N. G.; Geiger, W. E., *Chem. Rev.*, **1996**, *96*, 877-910; (b) Steckhan, E., *Top. Curr. Chem.*, **1987**, *142*, 1-69.
24. (a) Bjorn, A. University of Cincinnati, Cincinnati, Ohio, 2002; (b) Murata, Y.; Cheng, F.; Kitagawa, T.; Komatsu, K., *J. Am. Chem. Soc.*, **2004**, *126*, 8874-8875.
25. Noviadri, I.; Brown, K. N.; Fleming, D. S.; Gulyas, P. T.; Lay, P. A.; Masters, A. F.; Phillips, L., *J. Phys. Chem. B*, **1999**, *103*, 6713-6722.
26. SIR97; Altomare, A.; Burla, M. C.; Camalli, M.; Cascarano, G. L.; Giacovazzo, C.; Guagliardi, A.; Moliterni, A. G. G.; Polidori, G.; Spagna, R., *J. Appl. Crystallogr.*, **1999**, *32*, 115-119.
27. Betteridge, P. W.; Carruthers, J. R.; Cooper, R. I.; Prout, K.; Watkin, D. J., *J. Appl. Crystallogr.*, **2003**, *36*, 1487-1487.
28. Huebschle, C. B.; Sheldrick, G. M.; Dittrich, B., *J. Appl. Crystallogr.*, **2011**, *44*, 1281-1284.
29. Frisch, M. J. et al., *Gaussian 09, Revision D.01*, Gaussian, Inc.: Wallingford CT, 2009.
30. (a) Becke, A. D., *J. Chem. Phys.*, **1993**, *98*, 5648-5652; (b) Stephens, P. J.; Devlin, F. J.; Chabalowski, C. F.; Frisch, M. J., *J. Phys. Chem.*, **1994**, *98*, 11623-11627.
31. (a) Miertus, S.; Scrocco, E.; Tomasi, J., *Chem. Phys.*, **1981**, *55*, 117-129; (b) Barone, V.; Cossi, M.; Tomasi, J., *J. Chem. Phys.*, **1997**, *107*, 3210-3221; (c) Barone, V.; Cossi, M.; Tomasi, J., *J. Comput. Chem.*, **1998**, *19*, 404-417; (d) Tomasi, J.; Mennucci, B.; Cancès, E., *J. Mol. Struct.*, **1999**, *464*, 211-226.
32. (a) Schafer, A.; Huber, C.; Ahlrichs, R., *J. Chem. Phys.*, **1994**, *100*, 5829-5835; (b) Schafer, A.; Horn, H.; Ahlrichs, R., *J. Chem. Phys.*, **1992**, *97*, 2571-2577.
33. (a) Casida, M. E., In *Recent Advances in Density Functional Methods*. Chong, D. P., Ed. World Scientific: Singapore, 1995; p 155; (b) Stratmann, R. E.; Scuseria, G. E.; Frisch, M. J., *J. Chem. Phys.*, **1998**, *109*, 8218-8224.
34. (a) Tawada, Y.; Tsuneda, T.; Yanagisawa, S.; Yanai, T.; Hirao, K., *J. Chem. Phys.*, **2004**, *120*, 8425-8433; (b) Yanai, T.; Tew, D. P.; Handy, N. C., *Chem. Phys. Lett.*, **2004**, *393*, 51-57.
35. (a) Becke, A. D., *Phys. Rev. A*, **1988**, *38*, 3098-3100; (b) Lee, C. T.; Yang, W. T.; Parr, R. G., *Phys. Rev. B*, **1988**, *37*, 785-789.
36. (a) Gorelsky, S. I. AOMix, Program for Molecular Orbital Analysis; (b) Gorelsky, S. I.; Lever, A. B. P., *J. Organomet. Chem.*, **2001**, *635*, 187-196; (c) Gorelsky, S. I.; Solomon, E. I., *Theor. Chem. Acc.*, **2008**, *119*, 57-67.
37. Pratt, R. C.; Stack, T. D. P., *J. Am. Chem. Soc.*, **2003**, *125*, 8716-8717.
38. Dunn, T. J.; Webb, M. I.; Hazin, K.; Verma, P.; Wasinger, E. C.; Shimazaki, Y.; Storr, T., *Dalton Trans.*, **2013**, *42*, 3950-3956.
39. (a) Hansch, C.; Leo, A.; Taft, R. W., *Chem. Rev.*, **1991**, *91*, 165-195; (b) Hewage, J. S.; Wanniarachchi, S.; Morin, T. J.; Liddle, B. J.; Banaszynski, M.; Lindeman, S. V.; Bennett, B.; Gardinier, J. R., *Inorg. Chem.*, **2014**, *53*, 10070-10084; (c) Jovanovic, S. V.; Steenken, S., *J. Phys. Chem.*, **1992**, *96*, 6674-6679; (d) Lever, A. B. P., *J. Porphyrins Phthalocyanines*, **1999**, *3*, 488-499; (e) Masui, H.; Lever, A. B. P., *Inorg. Chem.*, **1993**, *32*, 2199-2201.
40. D'Alessandro, D. M.; Keene, F. R., *Chem. Soc. Rev.*, **2006**, *35*, 424-440.
41. (a) Hirotsu, M.; Kuwamura, N.; Kinoshita, I.; Kojima, M.; Yoshikawa, Y.; Ueno, K., *Dalton Trans.*, **2009**, 7678-7683; (b) Jozwiuk, A.; Wang, Z. D.; Powell, D. R.; Houser, R. P., *Inorg. Chim. Acta*, **2013**, *394*, 415-422; (c) Zolezzi, S.; Spodine, E.; Decinti, A., *Polyhedron*, **2002**, *21*, 55-59.
42. Robin, M. B.; Day, P., *Adv. Inorg. Chem. Radiochem.*, **1967**, *10*, 247.
43. Michel, F.; Hamman, S.; Thomas, F.; Philouze, C.; Gautier-Luneau, I.; Pierre, J. L., *Chem. Commun.*, **2006**, 4122-4124.
44. Lau, V. M.; Gorin, C. F.; Kanan, M. W., *Chem. Sci.*, **2014**, *5*, 4975-4979.
45. (a) Tedim, J.; Carneiro, A.; Bessada, R.; Patricio, S.; Magalhaes, A. L.; Freire, C.; Gurman, S. J.; Hillman, A. R., *J. Electroanal. Chem.*, **2007**, *610*, 46-56; (b) Silva, A. R.; Freire, C.; de Castro, B.; Freitas, M. M. A.; Figueiredo, J. L., *Microporous Mesoporous Mater.*, **2001**, *46*, 211-221.
46. (a) Andreiadis, E. S.; Jacques, P.-A.; Tran, P. D.; Leyris, A.; Charvarot-Kerlidou, M.; Jousset, B.; Matheron, M.; Pecaut, J.; Palacin, S.; Fontecave, M.; Artero, V., *Nature Chem.*, **2013**, *5*, 48-53; (b) XPS International, I., *Handbook of The Elements and Native Oxides*. 1999.
47. The spin densities on the nickel center of [Ni(Sal³⁻)]²⁻ when the CAM-B3LYP functional was used for optimization with no PCM model are as follows: R = CF₃: 25%; R = tBu: 16%; R = OMe: 4%; R = NMe₂: 2%.
48. Martin, R. L., *J. Chem. Phys.*, **2003**, *118*, 4775-4777.
49. (a) Bencini, A.; Fabbri, L.; Poggi, A., *Inorg. Chem.*, **1981**, *20*, 2544-2549; (b) Pinho, D.; Gomes, P.; Freire, C.; de Castro, B., *Eur. J. Inorg. Chem.*, **2001**, 1483-1493.
50. (a) Maki, A. H.; Davison, A.; Edelstein, N.; Holm, R. H., *J. Am. Chem. Soc.*, **1964**, *86*, 4580-4580; (b) Freire, C.; de Castro, B., *J. Chem. Soc., Dalton Trans.*, **1998**, 1491-1497; (c) Azevedo, F.; Carrondo, M.; Decastro, B.; Convery, M.; Domingues, D.; Freire, C.; Duarte, M. T.; Nielsen, K.; Santos, I. C., *Inorg. Chim. Acta*, **1994**, *219*, 43-54.
51. Solomon, E. I.; Gorelsky, S. I.; Dey, A., *J. Comput. Chem.*, **2006**, *27*, 1415-1428.

SYNOPSIS TOC (Word Style "SN_Synopsis_TOC"). If you are submitting your paper to a journal that requires a synopsis graphic and/or synopsis paragraph, see the Instructions for Authors on the journal's homepage for a description of what needs to be provided and for the size requirements of the artwork.

Nickel ($\text{Ni}(\text{Sal}^{\text{CF}_3})$) and copper ($\text{Cu}(\text{Sal}^{\text{CF}_3})$) complexes of an electron-deficient salen ligand were prepared, and their one-electron oxidized counterparts were studied using an array of experimental and theoretical methods. $\text{Ni}(\text{Sal}^{\text{CF}_3})$ undergoes ligand oxidation to afford a delocalized ligand radical, while $\text{Cu}(\text{Sal}^{\text{CF}_3})$ exhibits metal based oxidation to afford a Cu^{III} species.

